THE MEASUREMENT OF WOOD CELL PARAMETERS USING THE DISTANCE TRANSFORM

T. C. Peachey[1] *and C. F. Osborne*

Computer Imaging Group
Applied Physics Department
Chisholm Institute of Technology
P.O. Box 197 Caulfield East 3145
Victoria, Australia

(Received December 1988)

ABSTRACT

In this paper we present a new approach to the quantitative assessment of cell wood boundaries, using image processing techniques based upon the distance transform. It is demonstrated that the method produces the parameters of wall thickness and boundary perimeter using objective measures to estimate these parameters. Further, it is possible, using this technique, to segment the image of a sample of *Eucalyptus regnans* (mountain ash) into rays, lumens, and cell walls with minimum human intervention.

Keywords: Cell wall, distance transform.

INTRODUCTION

Characterization of the anatomical structure of wood is important in both the timber and the paper industries. Current methods revolve around the use of light microscopy and scanning electron microscopy with manual interpretation of the images. This interpretation suffers from several drawbacks: it may be slow, labor-intensive and introduce an element of subjectivity into the results. The subjectivity of operator assessment of these images is common to a large number of similar procedures. Examples are the classification of spermatozoa (Rowsell et al. 1987) and the evaluation of surface texture (Vandenberg and Osborne 1987) where automated techniques are currently being pursued.

Microtomed sections of wood cut in cross section, of thickness 12 μm, and stained with 1% aqueous safranin show under magnification the cell structure of the wood. Figure 1 shows a sample of *Eucalyptus regnans* (F. Muell). These stained samples were supplied by Mr. H. Ilic of the CSIRO Division of Building Research, who had found that the above stain was the most appropriate for these specimens. The cell lumens can be clearly distinguished; boundaries between cells are less obvious. When these boundaries can be discerned, it becomes possible to measure various parameters of the cells, such as cross-sectional area and perimeter. At present it is not possible to measure a large sample of cells because of the slowness of manual methods. In this paper we describe an automated imaging system for measuring wood cells.

SURVEY OF PREVIOUS METHODS

For delineation of cell boundaries using computer image processing techniques, several standard edge detectors are available (Gonzalez and Wintz 1987; Levine

[1]Also at MCOR, Footscray Institute of Technology, P.O. Box 64 Footscray 3011, Victoria, Australia.

Wood and Fiber Science, 22(4), 1990, pp. 388–403

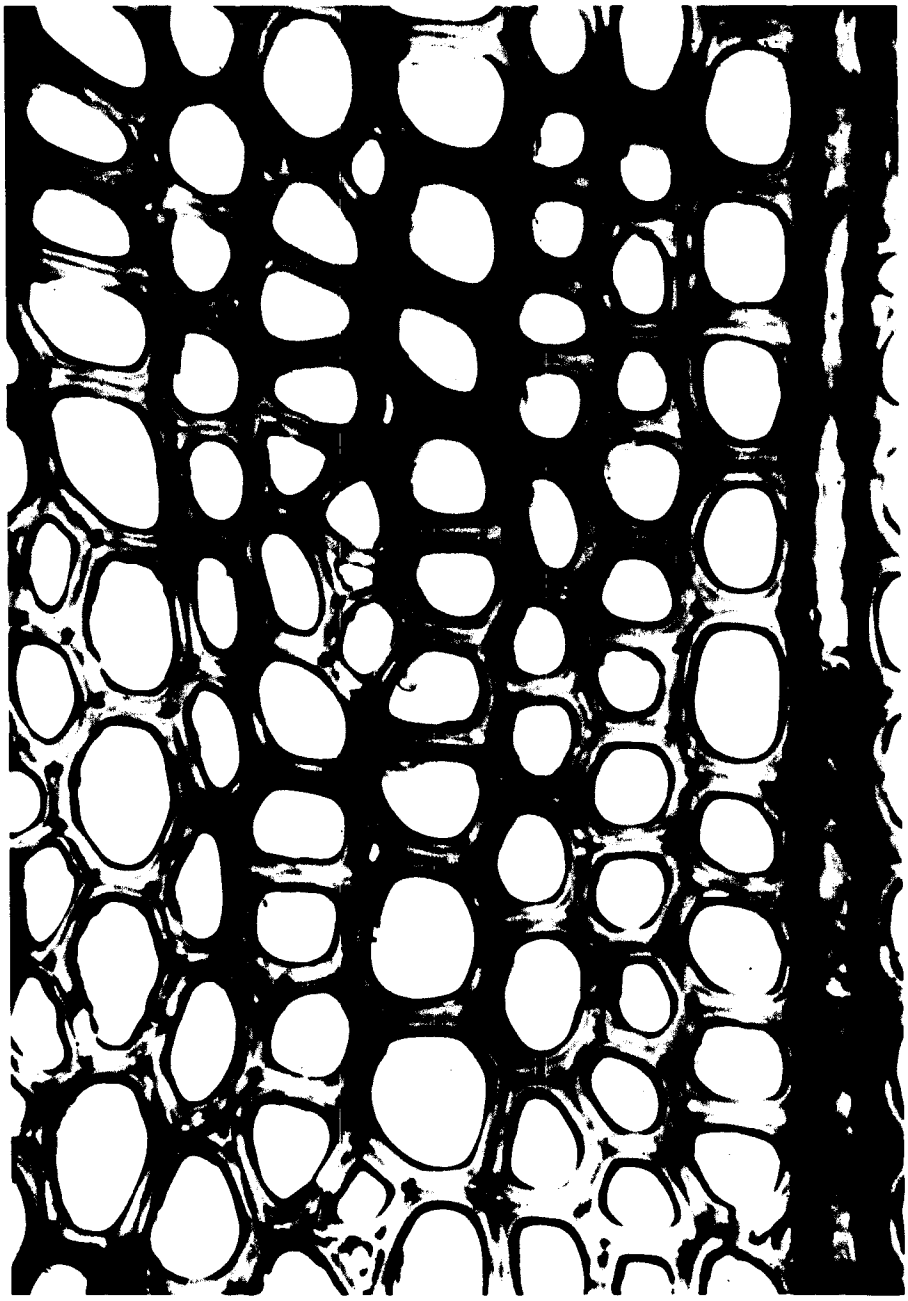

FIG. 1. Image of wood section.

1985). Edges tend to be defined to match specific imaging tasks. Generally, edges are acknowledged to be represented by coherent changes in gray level between local regions, which themselves are defined by locally constant values. Clearly, objects with textured surfaces present problems in edge definition since the surface

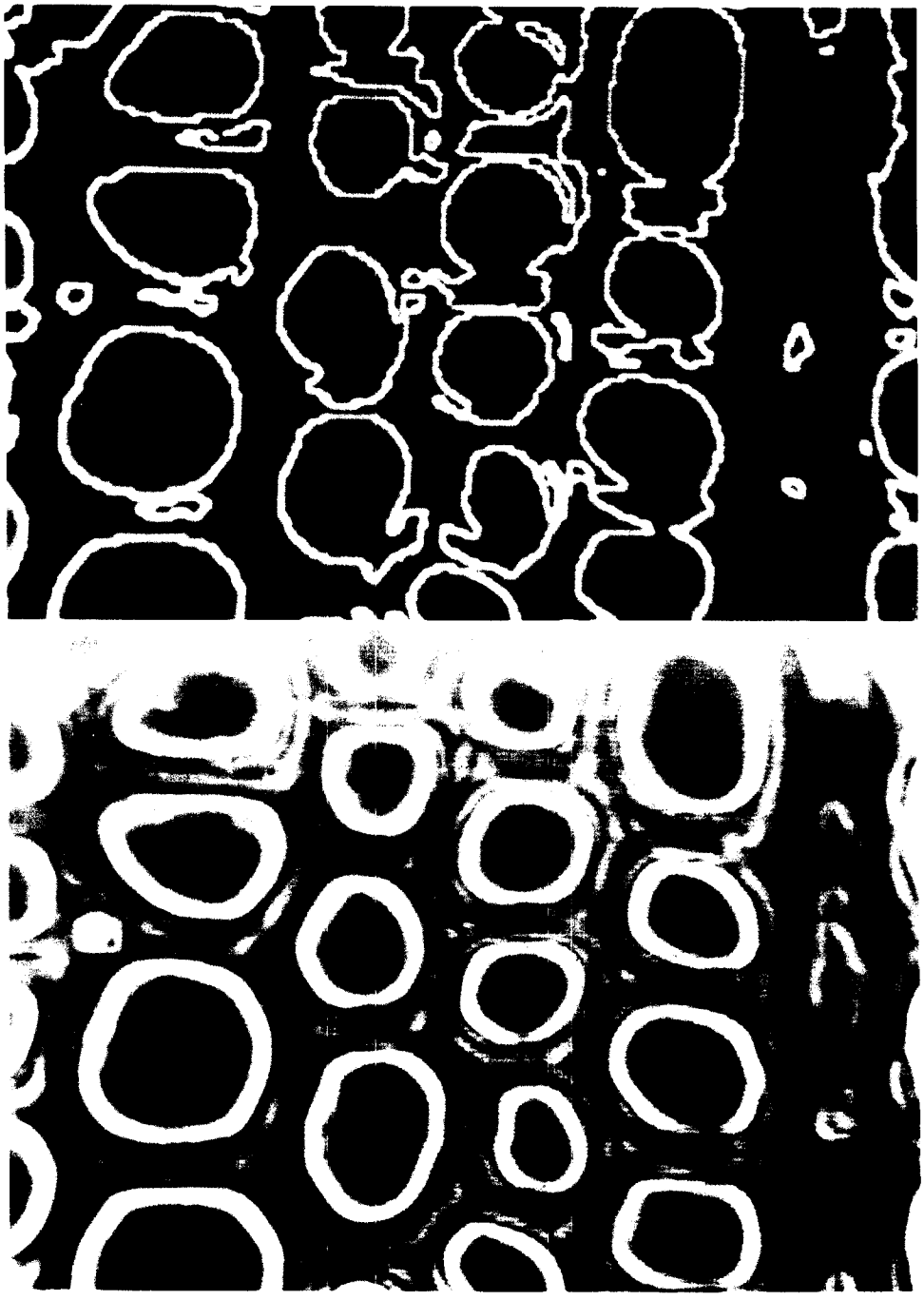

FIG. 2. (a) Robert's edge map of original image. (b) Sobel's edge map of original image. (c) Laplacian edge map of original image.

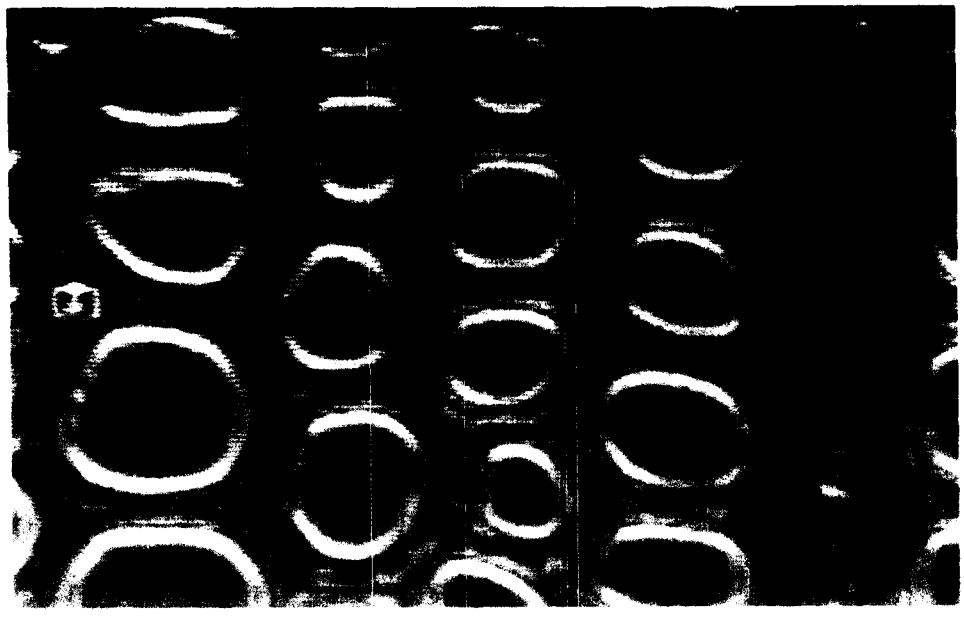

texture may contain many edges over fine scale dimensions. Similarly if the edges are weak, we can expect problems. In order to find edges, the image is first digitized into discrete "gray levels" at discrete "pixels." We write g_{ij} for the gray level of the pixel in the ith row and jth column. There are a number of methods that are available to enhance edge behavior and these are as follows:

(1) Subtraction of misregistered images: Small displacements in i and j (by say, 1 pixel) form a crude partial derivative in each direction. Since edges are defined by changes in gray level, the gray level gradient maps edge boundaries.
(2) Smoothing of an image (blurring) followed by subtraction from the original image enhances the edges.
(3) Local convolution using masks that approximate gradients can find edges.

The Roberts edge detector calculates for each pixel a discrete version of |grad g|, namely $|g_{i+1,j} - g_{i,j}| + |g_{i,j+1} - g_{i,j}|$. The results of this operation on a section of the image of Fig. 1 is displayed in Fig. 2a.

The Sobel operator is similar to the Roberts, except that a larger "mask" is used, more pixels around (i,j) are used to calculate the new value at (i,j), and so the method is less sensitive to noise. More precisely, the Sobel operator replaces g_{ij} by the convolution of the image with masks of the form

$$\text{a.}\begin{matrix} 1 & 0 & -1 \\ 2 & 0 & -2 \\ 1 & 0 & -1 \end{matrix} \qquad \text{b.}\begin{matrix} -1 & -2 & -1 \\ 0 & 0 & 0 \\ 1 & 2 & 1 \end{matrix}$$

$$\text{c.}\begin{matrix} 0 & -1 & -2 \\ 1 & 0 & -1 \\ 2 & 1 & 0 \end{matrix} \qquad \text{d.}\begin{matrix} -2 & -1 & 0 \\ -1 & 0 & 1 \\ 0 & 1 & 2 \end{matrix}$$

Thus if mask (a) is used, then g_{ij} is replaced by $g_{i-1,j-1} - g_{i-1,j+1} + 2(g_{i,j-1} - g_{i,j+1}) + g_{i+1,j-1} - g_{i+1,j+1}$. This has the effect of being non-zero when we have vertical edges in the image.

These 5-level masks differentially weight the center axis of the mask in the direction in which the gray level difference is being sought. There are 8 such masks, or 4 masks with sign differentiation of line direction. Again, the gradient magnitude is the largest of the four values returned at each point. The local angle of the edge ($\pm 22.5°$) is also determined using these masks.

Applying these masks to the same section of the original image yields the edge map as shown in Fig. 2(b). Fig. 2(c) shows the effect of applying a Laplacian mask to the same section. The Laplacian mask is shown below.

$$\begin{matrix} 0 & 1 & 0 \\ 1 & -4 & 1 \\ 0 & 1 & 0 \end{matrix}$$

This mask is extremely sensitive to noise and produces a response of variable strength depending on whether the data within the mask is an edge, or a point (4 times the edge response), a line end (3 times the edge), or a line (2 times the edge).

The results shown in Fig. 2 demonstrate that these edge detection methods clearly delineate the lumen boundaries but give only a patchy and confused indication of the cell boundaries. For an image with greater constrast in the middle lamellae, edge detection may give satisfactory results; but production of such images is not feasible for routine sampling of wood. Since cell boundaries cannot always be detected (if at all), we decided to assume that cell boundaries are midway between lumens of adjacent cells. Where the boundaries can be seen, Fig. 1 suggests that this is a reasonable approximation at least for this image.

In section 2 we describe a method that enables us to tessellate the image in the manner described above. In section 3 we discuss the technical details of the implementation of the ideas discussed in 2. In section 4 we discuss the performance of the system and in section 5 we give the results of our method and compare it with the edge finding methods discussed above.

THE DISTANCE TRANSFORM

To calculate cell boundaries under the assumption that the cell boundaries are midway between lumens of adjacent cells, we need to know for each pixel in the image which lumen is closest. Exact computation would be slow, so we have used an approximate technique known as the "distance transform" described below, and more fully in Rosenfeld and Pfaltz 1966; Borgefors 1984, 1985. This is a local operation; the distance for each pixel from the lumens is estimated using the distances of neighboring pixels. The method is fast because it uses only integer addition and integer comparisons.

$$\begin{matrix} & c_{2,1} & & c_{2,-1} & & & 11 & & 11 & \\ c1,2 & c_{1,1} & c_{1,0} & c_{1,-2} & 11 & 7 & 5 & 7 & 11 \\ & c_{0,1} & c_{0,0} & & & 5 & 0 & & \end{matrix}$$

FIG. 3. Distance transform masks.

More precisely, suppose that c_{ij} is the "mask" array shown in Fig. 3a with $c_{0,0}$

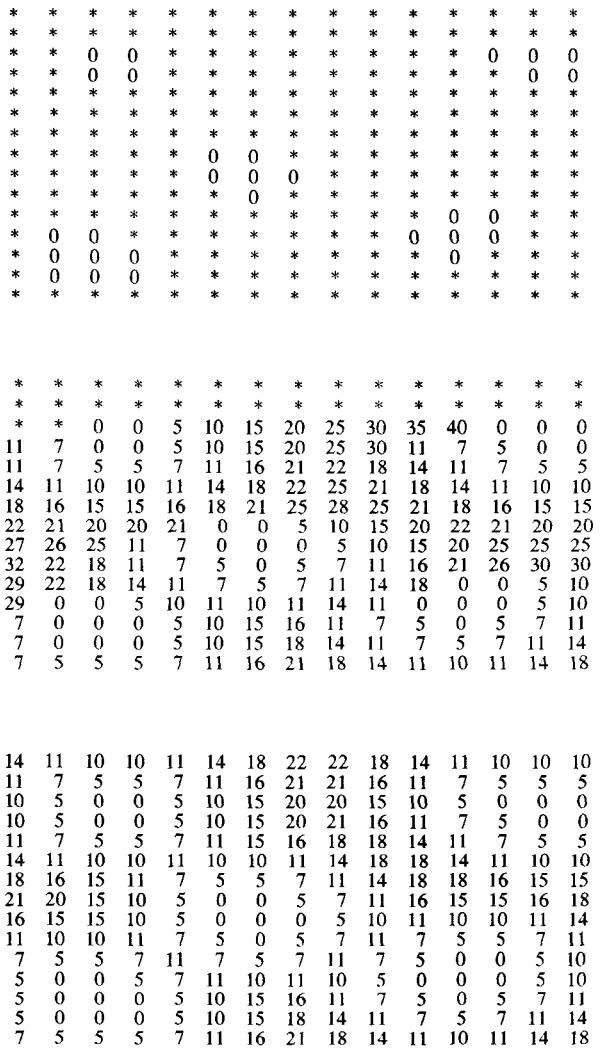

FIG. 4. (a) Test "Lumen" image. (b) Forward transform image. (c) Backward transform image.

= 0. For each pixel in the image, assign a value d_{ij} which is 0 if that pixel is in a lumen and some large number otherwise. Then working by rows from the top left pixel to the bottom right one, we replace d_{ij} by the minimum of $d_{i-r,j-s} + c_{r,s}$ taken over all $c_{r,s}$ in the mask. This is the "forward pass."

To complete the process, we need a "backward pass." For each pixel from the bottom right to the top left, we replace the current d_{ij} by the minimum of $d_{i+r,j+s} + c_{r,s}$. For example, in Fig. 4a the zeros represent lumen pixels and the stars represent the "large number" 255. Using the 5-7-11 mask of Borgefors, Fig. 3b, the forward pass, converts the image of Fig. 4a to that of 4b. And then the backward pass yields Fig. 4c. The final array gives distances from the pixels labelled 0, assuming that the pixel dimension is 5 units.

Use of the distance transform does not give exact distance values. However Borge-

0	0	0	0	0	0	0	0	0	0	0	0	0	0	0
0	0	0	0	0	0	0	0	0	0	0	0	0	0	0
0	0	1	1	0	0	0	0	0	0	0	0	2	2	2
0	0	1	1	0	0	0	0	0	0	0	0	0	2	2
0	0	0	0	0	0	0	0	0	0	0	0	0	0	0
0	0	0	0	0	0	0	0	0	0	0	0	0	0	0
0	0	0	0	0	0	0	0	0	0	0	0	0	0	0
0	0	0	0	0	3	3	0	0	0	0	0	0	0	0
0	0	0	0	0	3	3	3	0	0	0	0	0	0	0
0	0	0	0	0	0	3	0	0	0	0	0	0	0	0
0	0	0	0	0	0	0	0	0	0	0	4	4	0	0
0	5	5	0	0	0	0	0	0	0	4	4	4	0	0
0	5	5	5	0	0	0	0	0	0	0	4	0	0	0
0	5	5	5	0	0	0	0	0	0	0	0	0	0	0
0	0	0	0	0	0	0	0	0	0	0	0	0	0	0

1	1	1	1	1	1	1	1	2	2	2	2	2	2	2
1	1	1	1	1	1	1	1	2	2	2	2	2	2	2
1	1	1	1	1	1	1	1	2	2	2	2	2	2	2
1	1	1	1	1	1	1	1	2	2	2	2	2	2	2
1	1	1	1	1	1	3	3	3	2	2	2	2	2	2
1	1	1	1	1	3	3	3	3	3	2	2	2	2	2
1	1	1	3	3	3	3	3	3	3	3	2	2	2	2
5	3	3	3	3	3	3	3	3	3	3	4	4	4	4
5	5	3	3	3	3	3	3	3	3	4	4	4	4	4
5	5	5	3	3	3	3	3	3	3	4	4	4	4	4
5	5	5	5	3	3	3	3	3	4	4	4	4	4	4
5	5	5	5	5	3	3	3	4	4	4	4	4	4	4
5	5	5	5	5	5	5	3	4	4	4	4	4	4	4
5	5	5	5	5	5	5	4	4	4	4	4	4	4	4
5	5	5	5	5	5	5	5	4	4	4	4	4	4	4

FIG. 5. Tesselation of an image. (a) Test "lumen" image. (b) Tesselated image.

fors (1985) has shown that with the 5-7-11 mask, the maximum error is approximately 2%. We have modified the algorithm. For each pixel when deciding the minimum value of d + c, we also record the neighboring pixel which gave that minimum value, we pass to the current pixel an integer s_{ij} specifying the closest lumen. The final array of values of s_{ij} gives a "tessellation" of the original image into regions each of which is composed of those pixels closest to a certain lumen. For example in Fig. 5a, we start with lumens labelled 1 to 5 and Fig. 5b gives the completed tessellation.

The interested reader is referred to the seminal paper of Borgefors (1985) for further information; and in a future publication the authors will describe more fully their algorithms and the limitations of their system.

DESCRIPTION OF THE SYSTEM

An imaging system for analyzing wood cells (henceforth called WOODY) was developed by the image processing group in the Department of Applied Physics at Chisholm Institute of Technology. Images are taken from a microscope via a Hanimatsu Charge Coupled Device (CCD) camera and stored on a PC Vision card using proprietary software. We describe the image processing of the system in terms of its effect on the image of Fig. 1.

The dark vertical stripe is a ray cell and must be identified by the system. Other features, such as intracellular spaces, avail pharenchyma, and resin canels are of importance at different magnification levels and could be eliminated using morphology techniques that are different from the work considered here. This elimination process is not relevant to the present task. This is achieved by interactive

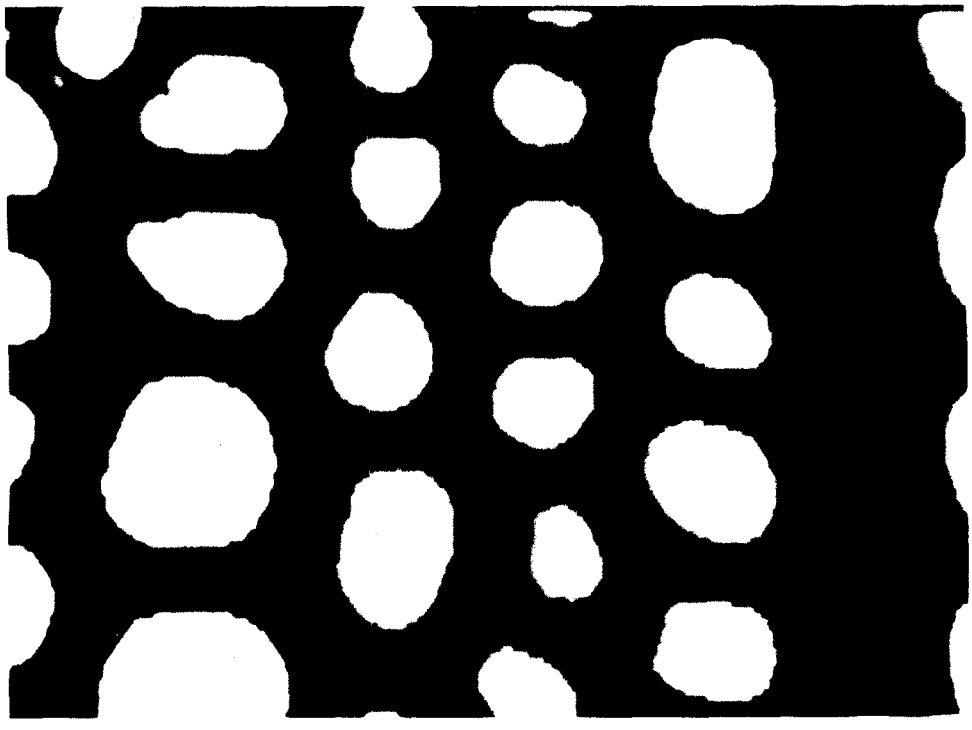

FIG. 6. Image with some areas misclassified.

thresholding; all pixels with gray levels below a certain threshold value are converted to black. This assumes that rays are in general darker than other parts of the image, so that substantial groups of black pixels will represent ray cells. At the same time pixels with gray level greater than a second threshold are judged to be lumen pixels and are converted to white. The result of this dual thresholding is shown in Fig. 6. Hereafter we refer to three types of pixels: ray pixels, lumen pixels and wall pixels. At this stage ray pixels have gray level $g_{ij} = 0$, lumen pixels have $g_{ij} = 255$, and wall pixels $0 < g_{ij} < 255$.

Clearly some pixels in Fig. 6 have been misclassified. These pixels are indicated by the arrows. WOODY allows operator intervention to modify patches of the image where substantial parts have fallen into the wrong category. However, minor noise is corrected by a process of "erosion" and "dilation," which we now discuss. The interested reader is referred to Serra (1982) for more details concerning morphological ideas related to erosion and dilation.

To correct the ray pixels, we assume that rays are long vertical structures. The image must be oriented so that rays are vertical. A vertical erosion is performed that converts all ray pixels to wall pixels unless they are preceded in that column by, say n ray pixels. Then a vertical dilation adds n ray pixels before all remaining ray pixels. The combined operation does not change a vertical column of more than n contiguous ray pixels but eliminates shorter sequences of ray pixels. The overall effect is to eliminate black regions with a vertical dimension not exceeding n.

To correct the pixels that have been wrongly labelled as lumens, we erode and

```
* * * * * * * * * * * * * * *
* * * * * * * * * * * 0 0 * *
* * 0 0 * * * * * * * 0 * * *
* 0 0 0 0 * * * * * * * * * *
* 0 0 0 0 * * * * * * * * * *
* * 0 0 0 0 * * * * * * * * *
* * * 0 0 0 * * * * * * * * *
* * * * 0 0 * 0 * * * * * * *
* * * * * * * * * 0 * * * * *
* * * * * * * * * 0 0 0 0 * *
* * * * * * * * 0 0 0 0 0 * *
* * * * * * * * * 0 0 0 0 * *
* * * * * 0 * * * * 0 0 * * *
* * * * * * * * * * * * * * *
```

```
0 0 0 0 0 0 0 0 0 0 0 0 0 0 0
0 0 0 0 0 0 0 0 0 0 0 5 5 0 0
0 0 5 5 0 0 0 0 0 0 0 5 0 0 0
0 5 7 7 5 0 0 0 0 0 0 0 0 0 0
0 5 7 10 5 0 0 0 0 0 0 0 0 0 0
0 0 5 7 7 5 0 0 0 0 0 0 0 0 0
0 0 0 5 7 5 0 0 0 0 0 0 0 0 0
0 0 0 0 5 5 0 5 0 0 0 0 0 0 0
0 0 0 0 0 0 0 0 0 0 5 0 0 0 0
0 0 0 0 0 0 0 0 0 3 7 5 5 0 0
0 0 0 0 0 0 0 0 5 7 11 10 5 0 0
0 0 0 0 0 0 0 0 0 5 6 6 5 0 0
0 0 0 0 0 5 0 0 0 0 5 5 0 0 0
0 0 0 0 0 0 0 0 0 0 0 0 0 0 0
0 0 0 0 0 0 0 0 0 0 0 0 0 0 0
```

```
* * * * * * * * * * * * * * *
* * * * * * * * * * * * * * *
* * * * * * * * * * * * * * *
* * 0 0 * * * * * * * * * * *
* * 0 0 * * * * * * * * * * *
* * * 0 0 * * * * * * * * * *
* * * * 0 * * * * * * * * * *
* * * * * * * * * * * * * * *
* * * * * * * * * * * * * * *
* * * * * * * * * * 0 * * * *
* * * * * * * * * 0 0 0 * * *
* * * * * * * * * * 0 0 * * *
* * * * * * * * * * * * * * *
* * * * * * * * * * * * * * *
```

```
18 16 15 15 16 18 21 25 29 33 38 43 47 48 49
14 11 10 10 11 14 18 22 27 32 36 40 42 43 44
11 7 5 5 7 11 16 21 25 29 33 36 37 38 40
10 5 0 0 5 10 14 18 22 27 30 31 32 33 36
10 5 0 0 5 7 11 16 21 26 25 26 27 29 32
11 7 5 0 0 5 10 15 20 21 20 21 22 25 28
14 11 7 5 0 5 10 15 18 16 15 16 18 21 25
18 14 11 7 5 7 11 16 14 11 10 11 14 18 21
21 18 14 11 10 11 14 14 11 7 5 7 11 14 18
25 21 18 16 15 16 16 11 7 5 0 5 7 11 16
28 25 22 21 20 20 15 10 5 0 0 0 5 10 15
32 29 27 26 25 21 16 11 7 5 0 0 5 10 15
36 33 32 31 27 22 18 14 11 7 5 5 7 11 16
40 38 37 33 29 25 21 18 14 11 10 10 11 14 18
44 43 40 36 32 28 25 21 18 16 15 15 16 18 21
```

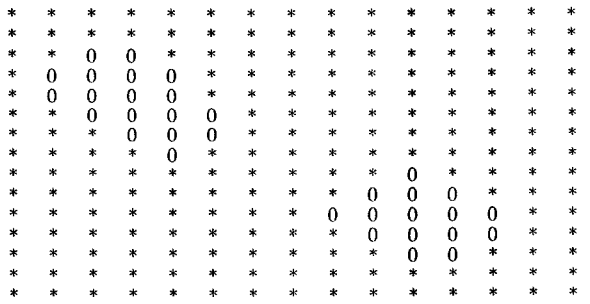

FIG. 7. (a) Test image. (b) Distance map. (c) Erosion. (d) Distance map. (e) Final image.

restore the lumen regions. This time, however, the process is two-dimensional. Using a distance transform, the distance of each lumen pixel from the wall regions is calculated. Those pixels for which this distance is less than some value, say m, are converted to wall status. Then a distance transform is again performed to give distances from these new lumens. Pixels within a distance m of the lumens are converted back to lumen pixels. This eliminates lumen regions with a minimum diameter of less than 2m.

Take for example, Fig. 7a, which shows an array where the 2 large connected sets of zeros represent lumens and the other zeros are artifacts to be eliminated. A distance transform into the lumens is shown in Fig. 7b and erosion with m = 6 gives Fig. 7c. Dilation of 6 units on the lumens gives the result shown in Fig. 7e using the distance transform of Fig. 7d.

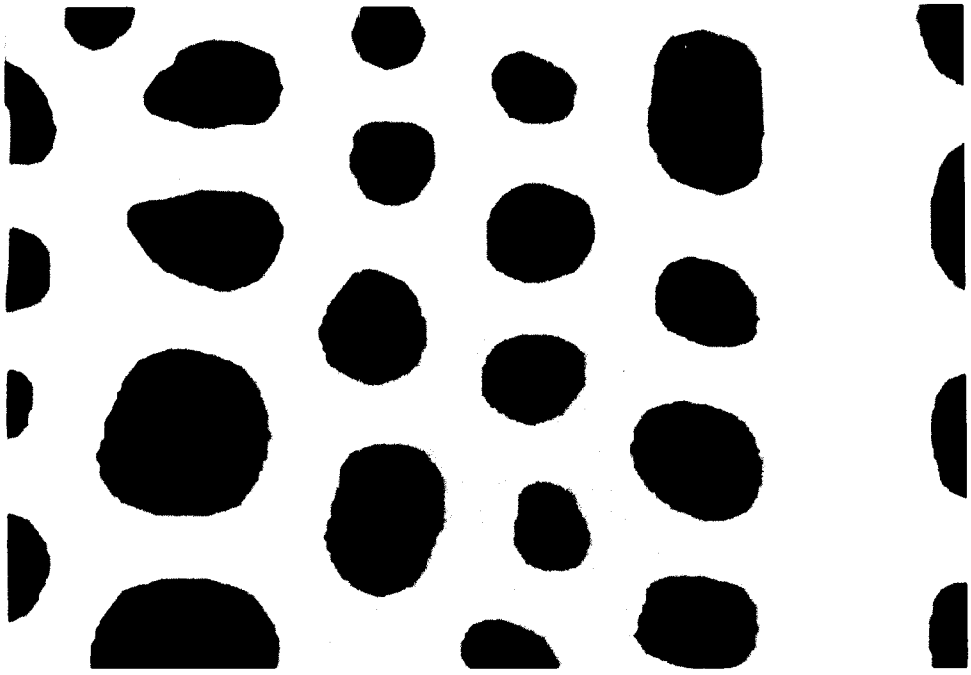

FIG. 8. Wood image with rays and noise removed.

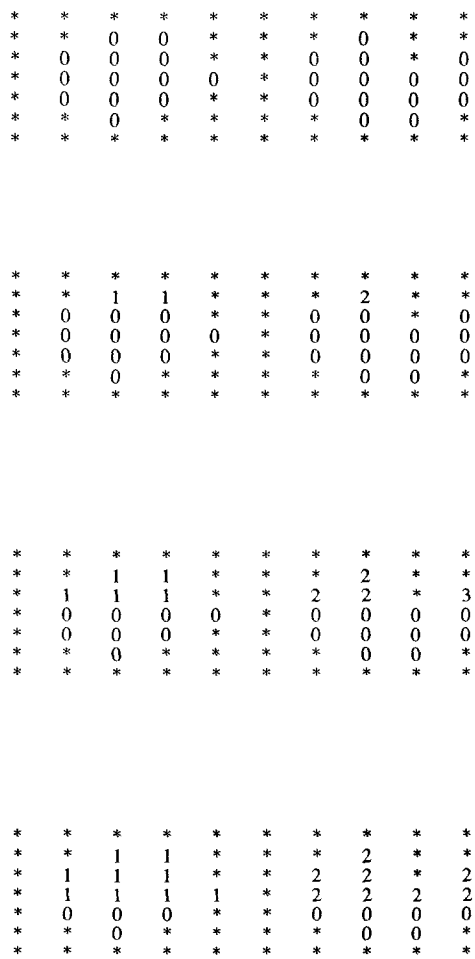

FIG. 9. (a)–(d) Steps in labelling lumens.

For the image of Fig. 6, ray pixels were adjusted with a vertical erosion and dilation of 60 pixel units, and lumen with a two-dimension erosion and dilation of 2 pixel units. The resulting image is shown in Fig. 8.

The next stage is to identify and label the separate lumens. The algorithm used considers each unbroken row of lumen pixels. If the row is adjacent to an earlier such row, then these pixels are all assigned a lumen number the same as that assigned to the earlier row. Otherwise the row is considered to be the first row in a new lumen and assigned the next lumen number. Figure 9 shows various stages in this process. The last stage shown illustrates a problem: regions originally identified as separate lumens may turn out to be part of the same lumen. The algorithm detects this situation and adjusts accordingly.

With the lumens labelled, a distance transform calculates the distance of all other pixels, simultaneously assigning to each pixel the lumen number of the closest lumen. The distance transform is shown in Fig. 10, and the corresponding tessellation in Fig. 11. Each region of the tessellation approximately corresponds

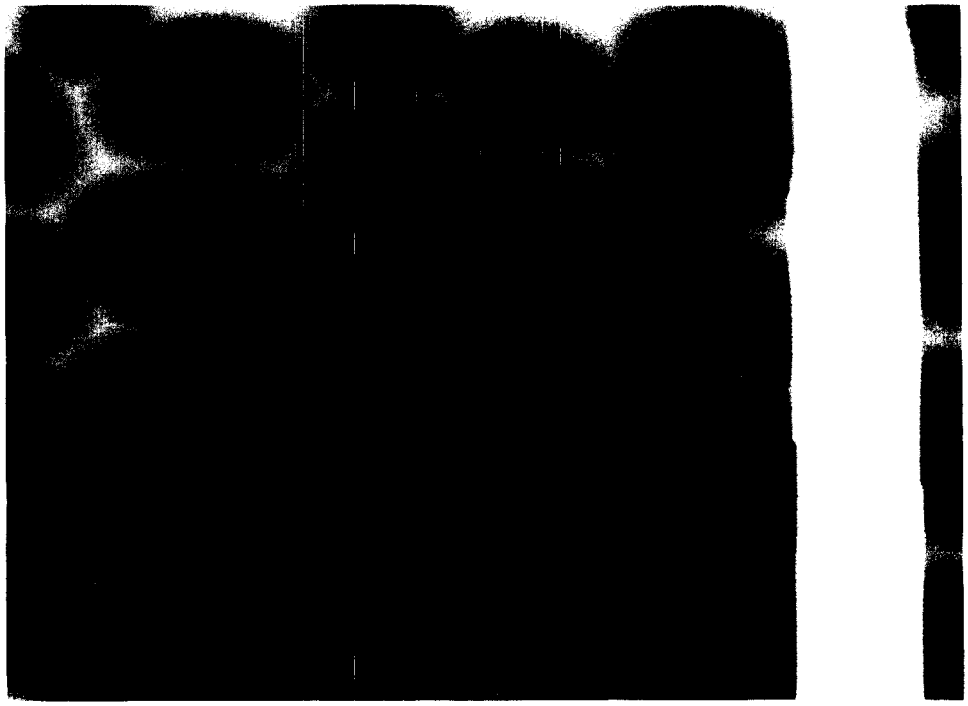

FIG. 10. Distance map.

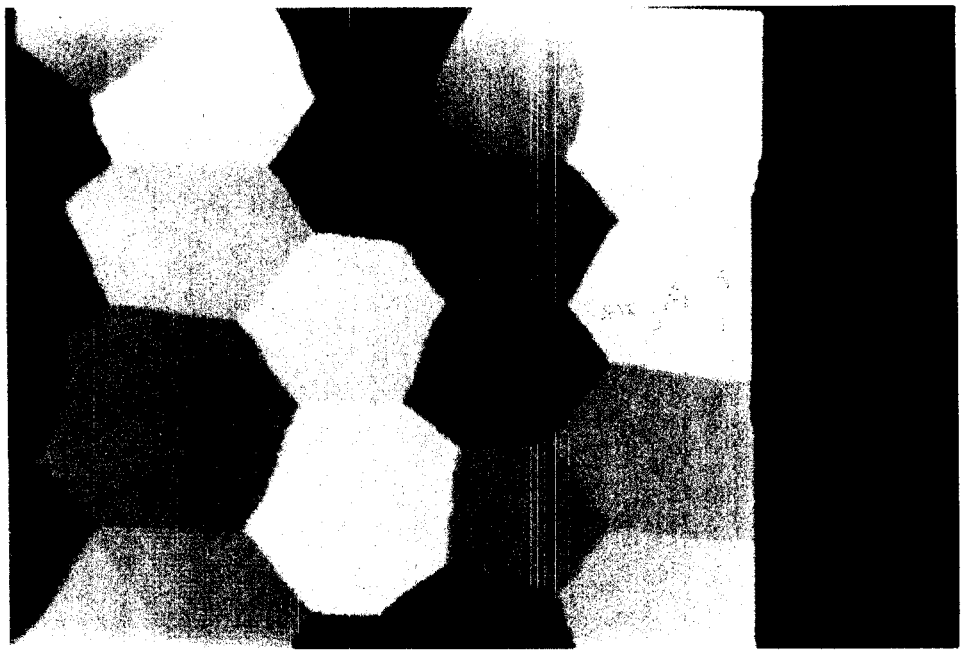

FIG. 11. Tessellation of wood.

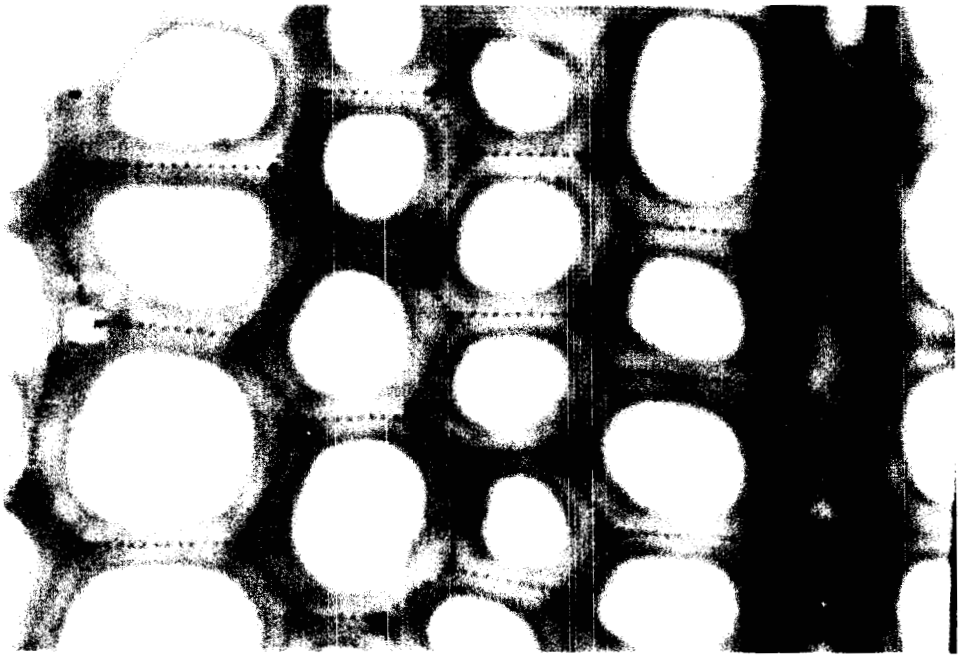

FIG. 12. Reconstruction of cell boundaries.

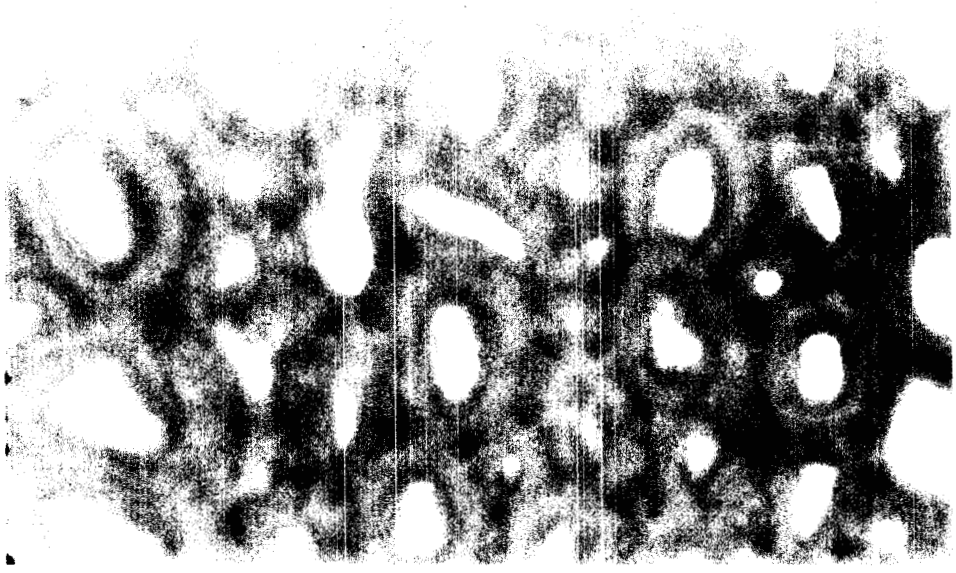

FIG. 13. Image where thresholding cannot obtain good segmentation.

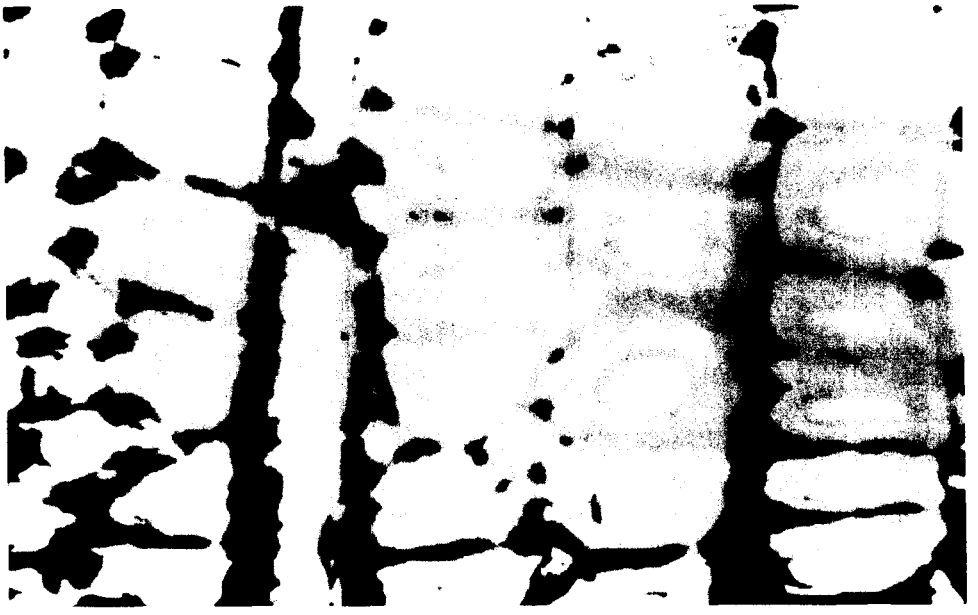

FIG. 14. Attempts to remove rays.

to a wood cell. Counting pixels gives the cross-sectional area. Further, the distance value for pixels on the boundary give the cell-wall thickness at that point. The system calculates maximum, minimum, and mean cell-wall thickness for each complete cell within the range.

To determine cell perimeter, a polygonal model is used. The cell corners are identified as points in the image where pixels of 3 different cells are in contact. These points are joined by straight line segments to give the polygonal cell boundary; cell perimeter is computed as the sum of these line segments. Fig. 12 shows the polygons superimposed on the original image. A "shape factor" defined by

$$s = \frac{(\text{perimeter})^2}{4\pi(\text{area})}$$

is also calculated for each cell. This measure is 1 for a circular disc and increases with deviation from circularity.

PERFORMANCE OF THE SYSTEM

WOODY was coded in C for execution on an MS-DOS microcomputer. Execution time for the 256 × 256 pixel image was 179 seconds using a 5-7-11 distance transform. The computer used was an IBM XT with a clock speed of 8 MHz. On current AT systems, the program takes considerably less time. A full screen image (512 × 512 pixels) will take proportionately longer. A simpler distance transform such as the 3–4 transform of Borgefors (1984) approximately halves execution time. This execution time was measured from the time that the operator decided on threshold values.

For the image of Fig. 1, Fig. 12 shows that the final polygonal models give a reasonable fit to the cell structure in most cases. An exception occurs at the junction

TABLE 1. *Statistics derived from the image.*

Cell	Lumen size (pixels)	Total size (pixels)	Cell wall				Perimeter (pixel)	No. of sides	Shape factor
			Area (pixel)^2	Mean width (pixel)	Max. width (pixel)	Min. width (pixel)			
6	2,021	4,545	2,524	12.2	18.2	9.0	255.3	7	1.14
8	1,115	3,182	2,067	12.7	18.4	9.4	210.7	6	1.11
10	897	2,642	1,745	11.6	15.0	8.0	195.0	6	1.15
11	1,244	3,382	2,138	12.1	15.6	9.2	223.1	7	1.17
12	582	2,046	1,464	11.6	15.4	8.8	172.5	6	1.16
16	706	2,250	1,544	11.5	15.0	8.0	177.9	6	1.12
17	858	2,593	1,735	11.9	16.0	8.8	191.6	6	1.13
19	464	1,813	1,349	11.3	15.0	9.0	162.9	5	1.16
20	1,149	2,971	1,822	11.5	18.2	7.0	212.4	5	1.21
23	758	2,483	1,725	12.4	19.0	7.0	193.3	5	1.20

of the two polygons on the left of the image. Here a small indistinct lumen has not been detected. This shows how the final distribution of measurements may be biased against small cells. Further, deletion of this cell causes errors in the measurements of adjacent cells, especially in their maximum wall thickness.

Performance of the system is sensitive to the quality of the images and the species of wood. Figure 13 shows the result of thresholding an image of *Eucalyptus delegaterisis,* where the gray levels of the lumen are close to those of the cell wall. WOODY wrongly identifies lumen pixels as wall regions. In Fig. 14, an image of Ash Eucalyptus, the ray is not appreciably darker than the middle lamellae and a column of such lamellae will be wrongly classified as a ray.

RESULTS

WOODY yields measurements only for complete cells; cells in contact with the image boundary are ignored. For each complete cell, the system measures the area of the total cell cross-section, area of the lumen, and of the cell wall. Wall width is computed—the maximum, minimum, and mean width taken around the cell boundary. Also generated are the perimeter, the number of sides of the polygonal model for the boundary, and the shape factor. Results from the section of the image of Fig. 1 are given in Table 1. Analysis of the accuracy of such results will be presented in a future paper.

CONCLUSION

The wood cell imaging system WOODY, when applied to images of transverse sections of some wood, can successfully distinguish cells and estimate their boundaries. For each cell, it gives a range of estimates of basic cell parameters. In the current system, no attempt has been made to calibrate, so the results are qualitative. In a future paper, we will investigate the accuracy of results generated by this system used on a variety of species of wood. The system should produce reasonable accuracy, and we envisage that the program can be used as a research tool to produce the large data-base of wood properties that manual methods cannot provide.

At present, WOODY cannot handle all image types. The operator needs to

choose suitable images and is called upon to select threshold values. New techniques are needed to overcome these drawbacks and give a truly automatic system. With images for which cell lumens are clear, WOODY can be expected to identify the cell and provide reasonable approximation to the position of the edges of the cells. Human intervention is needed only at the initial thresholding stage.

ACKNOWLEDGMENTS

We wish to acknowledge the assistance in the field of image processing provided by Messrs. R. Van Schyndel, A. Rowsell, S. Vandenberg, and Dr. Imants Svalbe of the Chisholm Institute of Technology. Advice on wood morphology was given by Dr. B. Allender of AMCOR Industries and Drs. H. Ilic and R. Evans of the Division of Forestry and Forest Products, CSIRO. The images used were supplied by Dr. Ilic.

References

BORGEFORS, G. 1984. Distance transformations in arbitrary dimensions. Computer Vision, Graphics and Image Processing 27:321–345.

———. 1985. Distance transformations in digital images. FOA Report C 30401-El National Defence Research Institute.

GONZALEZ, R. C., AND P. WINTZ. 1987. Digital image processing, 2nd ed. Addison-Wesley.

LEVINE, M. 1985. Computer vision in man and machine. McGraw-Hill.

ROSENFELD, A., AND J. PFALTZ. 1966. Sequential operations in digital picture processing. J. Assoc. Comput. Mach. 13:471–494.

ROWSELL, A. L., I. D. SVALBE, C. F. OSBORNE, G. N. CLARKE, D. Y. LIV, AND H. W. G. BAKER. 1987. Objective assessment of sperm morphology using image analysis in 5th Conference of the Aust. Soc. of Reproductive Biology, Sydney.

SERRA, J. 1982. Image analysis and mathematical order. Academic Press.

VANDENBERG S., AND C. F. OSBORNE. 1987. I. D. Svalbe ed. Quantitative measurement of texture *in* 2nd National Symposium on Computer Image Processing (Automated Vision Technology) in Melbourne, Australia July 14–15.